Radio-loud active galactic nuclei at high redshifts and the cosmic microwave background

G. Ghisellini,[1]⋆ A. Celotti,[1,2,3] F. Tavecchio,[1] F. Haardt[4,5] and T. Sbarrato[1,4,6]

[1]*INAF – Osservatorio Astronomico di Brera, via E. Bianchi 46, I-23807 Merate, Italy*
[2]*SISSA, via Bonomea 265, I-34135 Trieste, Italy*
[3]*INFN – Sezione di Trieste, via Valerio 2, I-34127 Trieste, Italy*
[4]*DiSAT, Università degli Studi dell'Insubria, Via Valleggio 11, I-22100 Como, Italy*
[5]*INFN, Milano–Bicocca, Piazza della Scienza 3, I-20126 Milano, Italy*
[6]*European Southern Observatory, Karl-Schwarzschild-Str. 2, D-85748 Garching bei München, Germany*

ABSTRACT

The interaction between the emitting electrons and the cosmic microwave background (CMB) affects the observable properties of radio-loud active galactic nuclei (AGN) at early epochs. At high redshifts z, the CMB energy density [$U_{\mathrm{CMB}} \propto (1 + z)^4$] can exceed the magnetic one (U_{B}) in the lobes of radio-loud AGN. In this case, the relativistic electrons cool preferentially by scattering off CMB photons, rather than by synchrotron emission. This makes more distant sources less luminous in radio and more luminous in X-rays than their closer counterparts. In contrast, in the inner jet and the hotspots, where $U_{\mathrm{B}} > U_{\mathrm{CMB}}$, synchrotron radiation is unaffected by the presence of the CMB. The decrease in radio luminosity is thus more severe in misaligned (with respect to our line of sight) high-z sources, whose radio flux is dominated by the extended isotropic component. These sources can fail detection in current flux-limited radio surveys, where they are possibly underrepresented. As the cooling time is longer for lower energy electrons, the radio luminosity deficit due to the CMB is less important at low radio frequencies. Therefore, objects not detected so far at a few GHz could be picked up by low-frequency deep surveys, such as Low-Frequency Array and Square Kilometre Array. Until then, we can estimate the number of high-z radio-loud AGN through the census of their aligned proxies, i.e. blazars, since their observed radio emission arises in the inner and strongly magnetized compact core of the jet and it is not affected by inverse Compton scattering off CMB photons.

Key words: radiation mechanisms: non-thermal – BL Lacertae objects: general – quasars: general – radio continuum: general.

1 INTRODUCTION

Radio emission from jetted extragalactic sources associated with active galactic nuclei (AGN) is produced in two main distinct locations, i.e. the relativistic jet and the at most mildly relativistic radio lobes (including the hotspots), where jet material impacts on to the intergalactic and intracluster media, and its mechanical power is partly dissipated in a shock (e.g. Begelman, Blandford & Rees 1984; De Young 2002). Radiation is strongly enhanced at viewing angles close to the jet axis by relativistic beaming, and it becomes very faint, until undetectable, for large viewing angles. On the contrary, the slower expanding extended lobes emit almost isotropically. The lobes are usually detected in the radio band thanks to their optically

thin synchrotron emission, which is characterized by a relatively steep energy spectral index, $\alpha \gtrsim 0.7$ [$F(\nu) \propto \nu^{-\alpha}$]. The radio jet emission, instead, is modelled as the superposition of several (partially) self-absorbed synchrotron components, produced by more compact structures, giving rise to a flatter radio spectrum ($\alpha \lesssim 0.7$).

The idea of unification of all radio sources on the basis of our viewing angle dates back to Blandford & Rees (1978; see Urry & Padovani 1995 for a review). When our line of sight lies within an angle $\sim 1/\Gamma$ to the jet axis, where Γ is the jet bulk Lorentz factor, the beamed, flat radio flux dominates and the source is classified as a blazar. For larger viewing angles isotropic emission from the extended regions takes over, and we do observe a steep spectrum radio source. The '$1/\Gamma$' beaming angle provides an approximated but convenient way to relate the number density of the observed blazars to that of the underlying parent population. Indeed, as discussed in Volonteri et al. (2011; see also Ghisellini et al. 2013), for

⋆ E-mail: gabriele.ghisellini@brera.inaf.it

each observed blazar there must exist a number $N \simeq 2\Gamma^2$ of sources intrinsically similar, but pointing away from us. The spectrum of such population should be steep in the radio band, while at larger frequencies isotropic components (e.g. emission lines, accretion disc and host galaxy), usually – but not always – masked in blazars by the relativistically boosted jet emission, dominate.

Blazars are easily detectable up to high redshifts. Although relatively rare, their large fluxes in almost all electromagnetic bands make them detected in large-area flux-limited surveys. The spectral energy distribution (SED) of blazars is characterized by two broad humps, usually interpreted as the synchrotron and the inverse Compton (IC) emissions from a single distribution of highly relativistic electrons (Sikora, Begelman & Rees 1994; Ghisellini et al. 1998). At increasing bolometric luminosities, the peak of the two humps shifts to lower frequencies, and the high-energy hump becomes comparatively stronger (Fossati et al. 1998; Donato et al. 2001). This phenomenology suggests that hard X-ray and γ-ray surveys are particularly efficient in finding powerful blazars at high redshifts. Indeed, such expectations are confirmed by the all sky surveys carried out by the Burst Alert Telescope (BAT) on-board *Swift* (detecting blazars up to $z \sim 4$; see Ajello et al. 2009) and by the Large Area Telescope (LAT) on-board *Fermi* (detecting blazars up to $z \sim 3$; see e.g. Nolan et al. 2012).

In this work, we will consider the subclass of powerful radio sources, classified as FR II radio galaxies (Fanaroff & Riley 1974) and steep spectrum radio-loud quasars, where the relativistic jet is misaligned, and flat spectrum radio quasars, whose jet points at us. These AGNs are the most powerful persistent sources we know of, their jets carrying a power, in magnetic fields and particles, that can exceed 10^{47} erg s^{-1} (Celotti & Ghisellini 2008; Ghisellini 2010a,b; Fernandes et al. 2011). Estimates of the energy associated with large-scale extended structures yield to at least 10^{60}–10^{61} erg, shared amongst relativistic emitting electrons, magnetic fields and possibly protons of still unknown temperature (e.g. Blundell & Rawlings 2000; Croston et al. 2005; Belsole et al. 2007; Godfrey & Shabala 2013).

In powerful blazars, the synchrotron hump peaks at sub-mm frequencies, with a steep spectrum above. The rapidly declining nonthermal emission ($\alpha \gtrsim 1$) allows us to detect the accretion disc component. Fits with a standard Shakura & Sunyaev (1973) disc emission model (Calderone et al. 2013; Castignani et al. 2013) imply for all powerful blazars at $z > 2$ in the BAT and LAT catalogues, black hole (BH) masses in excess of 10^9 M$_\odot$ (Ghisellini et al. 2010b, 2011). This fact boosted interest in the search of powerful blazars at high z, as an efficient way to count supermassive BHs at early epochs. In this context, blazars' counts can be competitive with (mainly optical) searches for mostly radio-quiet quasars (i.e. the Sloan Digital Sky Survey, SDSS; York et al. 2000).

As already mentioned, for each detected blazar, there must exist other $\sim 2\Gamma^2$ misaligned sources with similar properties, including M. Typical values of Γ are between 10 and 15, so the very presence of a single blazar with a BH mass $M > 10^9$ M$_\odot$ already implies the existence of other $450(\Gamma/15)^2$ sources with similar masses. Should such sources have extended structures similar to those seen at lower redshifts, they could be easily detected – even at $z > 3$ – in radio surveys like the Faint Images of the Radio Sky (FIRST at 20 cm; White et al. 1997), characterized by a flux limit of 1 mJy at 1.4 GHz. Instead these sources appear to be at best underrepresented in the combined SDSS+FIRST survey (see Volonteri et al. 2011). The chain of arguments leading to the claimed deficit was the following: first, we established that all BAT blazars with $z > 2$ and an X-ray luminosity (in the 15–55 keV band) $L_X > 2 \times 10^{47}$ erg s^{-1} have $M > 10^9$ M$_\odot$. Then, we exploited the luminosity function of Ajello

et al. (2009) to find out the expected density of blazars of high L_X ($\gtrsim 10^{47}$ erg s^{-1}, presumably hosting a BH with $M \gtrsim 10^9$ M$_\odot$) in different redshift bins. To be conservative, we modified the Ajello et al. (2009) luminosity function above $z = 4$, introducing an exponential cutoff at larger redshifts. Adopting $\Gamma = 15$ as an average value (estimated by fitting the SED of all the BAT blazars with $z > 2$; Ghisellini et al. 2010a), we then computed the overall density of powerful radio-loud AGNs hosting a $M > 10^9$ M$_\odot$ BH, in different redshift bins. Finally, we compared this expected number density with the detections in the SDSS+FIRST survey, finding agreement at $z \lesssim 3$ and a deficit of at least a factor of 10 above.

Recently, we showed that the source B2 1023+25 at $z = 5.3$ is a blazar (Sbarrato et al. 2012; 2013). This object, present in the SDSS+FIRST survey, was studied by Shen et al. (2011) and is one of the only four sources detected in radio above $z > 5$ in the Shen et al. (2011) catalogue. For B2 1023+25, we estimated $M = (3 \pm 1.5) \times 10^9$ M$_\odot$ and a bulk Lorentz factor $\Gamma = 13$. If its viewing angle is indeed $< 1/\Gamma$, we expect other $\sim 340(\Gamma/13)^2$ radio sources in the SDSS+FIRST survey, while there are only three. Given the importance of verifying the true number density of massive BHs in the early Universe, we are urged to explain such a discrepancy.

Volonteri et al. (2011) discussed this issue, suggesting four possible causes: (i) the radio lobes become for some (yet unknown) reason weaker than expected at $z \gtrsim 3$, falling below the FIRST detection threshold; (ii) the average Γ is typically (again for unknown reasons) smaller than 10–15 at high redshifts, so that the factor $2\Gamma^2$ is much smaller than assumed; (iii) powerful misaligned radio sources at high redshifts do not enter the SDSS survey because of heavy obscuration in the optical, so that they lie below its detection threshold; (iv) missing identifications of extended radio structures associated with lobes of an AGN.

Whatever the reason is, we face the intriguing fact that 'something' must change for sources at $z \gtrsim 3$. This led us to assess the effects of the cosmic microwave background (CMB) on the radio properties of the extended structures of powerful sources, and here we present our findings. The idea of the CMB affecting the behaviour of radio-loud AGN dates back to the works by Felten & Rees (1967) and Rees & Setti (1968), and it was followed by Krolik & Chen (1991) to explain the prevalence of sources with steep radio spectra at high redshifts. Later, Celotti & Fabian (2004) demonstrated that the extended structures of high-z powerful radio sources could contribute significantly to the diffuse X-ray background, via IC scattering between radio emitting electrons and CMB photons, while more recently Mocz, Fabian & Blundell (2011) studied the evolution of the extended structure of a radio source calculating synchrotron and adiabatic losses, as well as IC losses on CMB photons, whose radiation energy density is larger at larger redshifts.

Here, we concentrate on the synchrotron emission from those relativistic electrons cooling mainly by scattering off CMB seed photons. Since the energy density of the CMB scales as $(1 + z)^4$, it may become larger than the typical magnetic energy density in radio lobes, enhancing the total radiative losses, and hence modifying the electron distribution function, especially at the largest energies. We will compute in detail how the CMB modifies the electron distribution in jets, hotspots and extended lobes, and how the radio emission from powerful radio-loud AGNs changes with redshift, allowing us to compare our results with observations.

In this work, we adopt a flat cosmology with $H_0 = 70$ km s^{-1} Mpc^{-1} and $\Omega_M = 0.3$.

2 RADIO GALAXIES AND THE CMB

2.1 The environment of radio galaxies at different epochs

At all redshifts, the extended structure of a radio source is due to the energy deposited by the jet once it impacts on to the intergalactic medium. Today, powerful radio sources can easily reach ~ 1 Mpc away from the central engine. These radio sources are often associated with poor clusters or groups, and 1 Mpc is larger than the core radius $r_c \sim 0.1$ Mpc of a typical cluster, where the density is estimated to be about $n_c \sim 10^{-3}$ cm^{-3} (e.g. Sarazin 2008). Out of the core radius, the gas density approximatively follows an isothermal profile, $n = n_c/[1 + (r/r_c)^2]$, resulting in $n \sim 10^{-5}$ cm^{-3} at $r \sim 1$ Mpc. Such density is ~ 30 times larger than the mean cosmic density of baryons today.

We do not know the typical sizes, masses and gas densities of *proto*-clusters that can host powerful radio sources at $z \gtrsim 3$. What we do know is that the large BHs ($M \gtrsim 10^9$ M$_\odot$) required some time to accrete their masses. As an example, assuming a Salpeter time of 40 Myr, the time needed by a 10^2 M$_\odot$ BH seed to reach 10^9 M$_\odot$ is $\simeq 930$ Myr. If the seed mass is one hundred times larger, the time required is still $\simeq 660$ Myr.

Such time-scales are long enough for an early AGN to fully develop the extended radio lobes. In fact, the far end of the jet, assumed to be advancing at ~ 10 per cent of the light speed, takes only 32 Myr to reach a distance of ~ 1 Mpc. As the proto-cluster may have not completely formed yet at such high z, it is likely that the density at 1 Mpc from the centre is similar to the average cosmic baryon density, i.e. $n_{Mpc} \sim 2 \times 10^{-5}[(1 + z)/4]^3$ cm^{-3}.

The above simple estimates show our point: at high redshifts, the medium at ~ 1 Mpc from a radio-loud AGN (where the jet dissipates its own energy) has a density that, by chance, is similar to the density of the intracluster medium at $r \sim 1$ Mpc today. As a consequence, radio lobes of similar power should have similar sizes. If the magnetic field is always around equipartition, it should have a similar value today and at $z \simeq 3$.

We can now study the physics of the interaction between the extended emission of a jet and the CMB in details.

2.2 Cooling rates

As the energy density of the cosmic microwave background is

$$U_{CMB} = aT_0^4(1 + z)^4 = 4.22 \times 10^{-13}(1 + z)^4 \text{ erg cm}^{-3}, \quad (1)$$

where $T_0 = 2.725$ K is the CMB temperature today, the value of a magnetic field in equipartition with U_{CMB} is

$$B_{CMB} = [8\pi U_{CMB}]^{1/2} = 3.26 \times 10^{-6}(1 + z)^2 \text{ G}. \quad (2)$$

At $z = 3$, we have $B_{CMB} = 52$ µG, and $B_{CMB} = 120$ µG at $z = 5$.

Relativistic electrons contained in a plasma where $B < B_{CMB}$ would preferentially cool down via IC, rather than synchrotron losses. Consequently, the radio emission is expected to be quenched, or severely weakened. In order to quantify the strength of such effect, we need first to consistently determine the particle energy distribution. We will do this under the simplifying hypothesis of continuous injection of fresh particles, and we will account for radiative and adiabatic cooling.

A further approximation is related to the fact that particles are likely injected (i.e. accelerated to relativistic energies) by shocks in the hotspots and from there they diffuse out to fill up the extended radio lobes. The particle energy distribution is therefore a function of the distance from the injection region. For simplicity, we evaluate

instead an average distribution, adopting a spatially averaged magnetic field. This can be thought as equivalent to observe the radio source with poor angular resolution.

With the above simplifying assumptions, the adiabatic and radiative cooling rates can be written as

$$\dot{\gamma}_{ad} = \frac{\gamma v_{exp}}{R} \equiv \frac{\gamma \beta_{exp}}{R/c}, \quad (3)$$

$$\dot{\gamma}_{rad} = \frac{4}{3} \frac{\sigma_T c \gamma^2}{m_e c^2}(U_B + U_{CMB} + U_s), \quad (4)$$

respectively, where v_{exp} is the expansion speed of the lobe and U_s is the energy density of synchrotron radiation as electrons cool also via the synchrotron self-Compton mechanism. For the conditions considered here, these latter radiative losses are significantly smaller than synchrotron and IC ones off CMB photons, and can be thus safely neglected.

For a given extended region of length-scale R, adiabatic losses exceed the radiative ones for particle Lorentz factors up to a value γ_{ad} given by

$$\gamma_{ad} = \frac{3m_e c^2 \beta_{exp}}{4R\sigma_T(U_B + U_{CMB})}$$

$$\approx \frac{7.2 \times 10^5 \beta_{exp,-1}}{(1 + z)^4 R_2(1 + U_B/U_{CMB})}. \quad (5)$$

Here, $R_2 = R/100$ kpc and $\beta_{exp,-1} = \beta_{exp}/0.1$.

Adiabatic losses ($\propto \gamma$) do not alter the shape of the injected electron distribution, while radiative losses ($\propto \gamma^2$) steepen it. In the presence of a constant injection rate of a power-law distribution,

$$Q(\gamma) \propto \gamma^{-s}, \quad (6)$$

the slope of the evolved electron distribution $N(\gamma)$ steepens by one unity for Lorentz factors $\gamma > \gamma_{rad}$, as long as the condition $\gamma_{rad} > \gamma_{ad}$ holds. The value of γ_{rad} is given by

$$\gamma_{rad} = \frac{3m_e c^2}{4\sigma_T c \Delta t \, U_{CMB}(1 + U_B/U_{CMB})}, \quad (7)$$

where Δt is the time elapsed since a particle is injected in the source and can be regarded as the time spent by the particle inside the extended region.

In the present context, the region itself could consist of many smaller subregions whose length-scale is of the order of the coherence length of the magnetic field, λ. Particles then follow a sort of random walk with mean free path $\approx \lambda$, before escaping the source. We can thus write

$$\Delta t \approx \frac{R}{c}\left(1 + \frac{R}{\lambda}\right) \quad (8)$$

and, in turn,

$$\gamma_{rad} \approx \frac{4.9 \times 10^6}{(1 + z)^4 R_2[(1 + R/\lambda)](1 + U_B/U_{CMB})}. \quad (9)$$

Cooling electrons emit at synchrotron frequency

$$\nu_{s,cool} \approx 3.6 \times 10^6 B \gamma_{rad}^2 \text{ Hz}$$

$$= \frac{1.8 \times 10^{15} B_{-5}}{\{(1 + z)^4 R_2[(1 + R/\lambda)](1 + U_B/U_{CMB})\}^2}. \quad (10)$$

If we assume $\lambda \sim 10$ kpc (Carilli & Taylor 2002; Celotti & Fabian 2004), we find that, for $B = 10$ µG, the main radiative coolant is synchrotron emission for $z \lesssim 1$, while at higher redshifts IC off

CMB photons dominates (see equation 2). For reference, at $z = 2$ ($z = 3$), the rest frame cooling frequency ν_s is 2 GHz (0.2 GHz).

2.3 Relativistic energy distribution of emitting particles

The time-dependent relativistic energy distribution $N(\gamma, t)$ (in cm^{-3}) of the emitting particles is calculated through a continuity equation, for a constant injection rate of fresh particles at rate $Q(\gamma)$ (in cm^{-3} s^{-1}), and assuming adiabatic and radiative cooling. Electrons emit synchrotron photons in the radio band, and IC in X/γ-rays.

The solution of the continuity equation is time dependent. For illustrative purposes, in the following, we will show results computed at time $t = \Delta t$ after the start of particle injection. We remind that Δt is the particle escape time from the source. Such characteristic time is approximately the time needed for the particle distribution to reach a stationary configuration. This is strictly true in the case of steady continuous injection lasting a time $\gg \Delta t$. We must note however that even in this case the particle distribution may never reach a stationary state, since source expansion most likely decreases the average magnetic field (see e.g. Mocz et al. 2011). With such caveat in mind, we can now compute particle distributions and the relative emission spectra. To do so, we further assume that the magnetic field is constant for a time Δt. At high energies, $\gamma \gtrsim \gamma_{\mathrm{rad}}$, we have

$$N(\gamma) \sim \int_\gamma \frac{Q(\gamma')}{\dot{\gamma}_{\mathrm{rad}}} \, d\gamma' \qquad (11)$$

where $N(\gamma) \equiv N(\gamma, \Delta t)$. As long as $U_{\mathrm{B}} \gg U_{\mathrm{CMB}}$, increasing U_{CMB} leaves $N(\gamma)$ unaltered. The high-energy emission increases, but the radio synchrotron flux stays constant. In contrast, when U_{CMB} exceeds U_{B}, $N(\gamma)$ is bound to decrease. This implies a constant high-energy flux – since the increase of U_{CMB} exactly compensate for the decrease of $N(\gamma)$ – while the (radio) synchrotron flux *decreases*.

At lower energies, $\gamma \lesssim \gamma_{\mathrm{rad}}$, radiative losses are negligible and hence $N(\gamma)$ has the very same slope of the injected distribution $Q(\gamma)$, and a normalization set by adiabatic losses and particle escape. If adiabatic losses prevail, then

$$N(\gamma) \sim \int_\gamma \frac{Q(\gamma')}{\dot{\gamma}_{\mathrm{ad}}} \, d\gamma', \qquad (12)$$

if instead escape dominates, then

$$N(\gamma) \sim \Delta t \, Q(\gamma). \qquad (13)$$

As long as adiabatic cooling dominates, $N(\gamma)$ becomes insensitive to changes of U_{CMB}. This means that at low radio frequencies, the same source will have the same luminosity for any U_{CMB}, i.e. independent of redshift. It should be noted, however, that this could happen at electron energies corresponding to the self-absorbed part of the synchrotron spectrum, and therefore the effect could be difficult to observe, unless γ_{rad} is significantly larger than the self-absorption energy. This latter circumstance may happen if the escape time is short, i.e. for a small source size.

In the following section, we will show a few examples of solutions of the continuity equation discussed above.

2.4 Examples of energy distributions

We assume our idealized source as homogeneous and spherical, with a homogeneous and tangled magnetic field filling it up. To highlight the role of the CMB in determining the observable properties of radio-loud AGNs, we assume that the structure and the basic intrinsic properties of the source are independent of redshift.

The size of the extended source is taken as $R = 100$ kpc. Relativistic electrons are injected throughout the source at constant rate, and we fix the magnetic field coherence length to 10 kpc. Finally, the entire source is assumed to expand at $\beta_{\mathrm{exp}} = 0.1$.
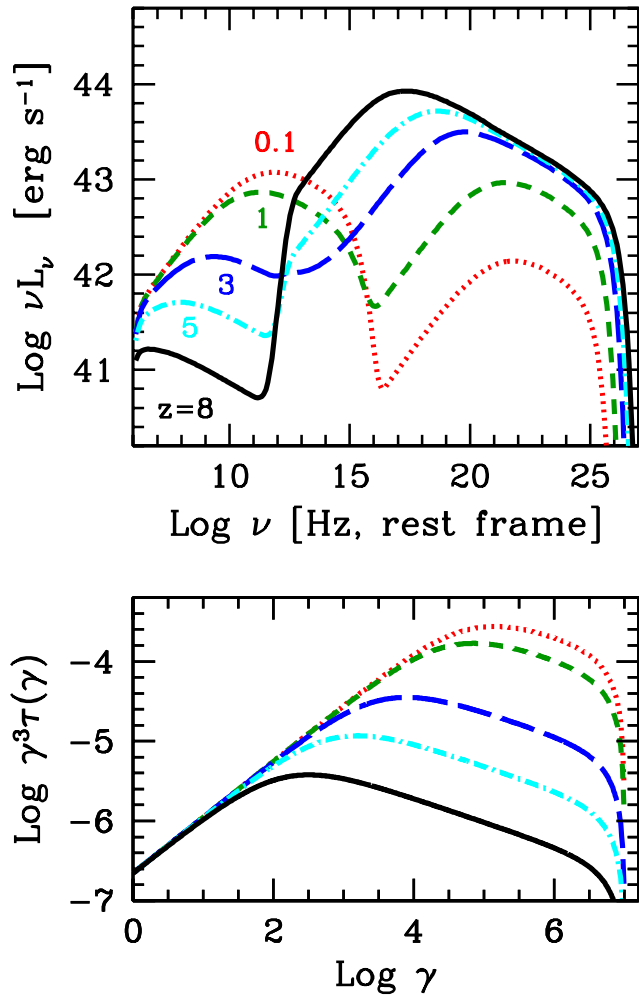
2.4.1 Single power-law injection

We start by assuming that electrons are injected throughout the source with a simple power-law distribution, i.e. $Q(\gamma) \propto \gamma^{-2.3}$ between $\gamma_{\min} = 1$ and $\gamma_{\max} = 10^7$ and $B = 10$ μG throughout the entire region. The assumed slope is within the range predicted by shock acceleration (e.g. Kirk & Duffy 1999) and what observed in real sources (e.g. Kataoka & Stawarz 2005). The power injected in relativistic electrons is always $P = 5 \times 10^{45}$ erg s^{-1}. This injected power yields – according to equations (12) and (13) – an energy content in relativistic electrons close to equipartition with the magnetic field energy: $\log(E_{\mathrm{B}}/\mathrm{erg}) = 59.8$ and $\log(E_{\mathrm{e}}/\mathrm{erg}) = 59.6$ (at $z = 0.1$), and $\log(E_{\mathrm{B}}/\mathrm{erg}) = 59.8$ and $\log(E_{\mathrm{e}}/\mathrm{erg}) = 59.5$ (at $z = 8$). The energy content in particles is not exactly the same at different z, but it decreases at large redshifts, since their cooling increases. We compute the electron density distribution and the generated SED as discussed above.

In the top panel of Fig. 1, we show the predicted SED of a source of equal intrinsic properties, but located at different redshifts. The bottom panel illustrates the corresponding electron distributions. The electron distribution is plotted as $\gamma^3 \tau(\gamma) = \sigma_{\mathrm{T}} R \gamma^3 N(\gamma)$, so that its peak corresponds to the Lorentz factor value that emits at the two peaks (synchrotron and IC) in the νL_ν photon distribution.

Fig. 1 allows us to appreciate the large evolution of the predicted SED as the redshift increases. IC cooling increases as $U_{\mathrm{CMB}} \propto (1 + z)^4$, and the corresponding losses, for the assumed parameters, become equal to the synchrotron ones at $z \simeq 0.75$ (see equation 2 for $B = 10$ μG). As the redshift increases, the source becomes more and more Compton dominated, as was pointed out by Celotti & Fabian (2004), who also emphasized the diffuse nature of the produced X-ray radiation. Celotti & Fabian (2004) argued that such diffuse high-energy emission could represent a large part of the *truly diffuse* X-ray background.

As already mentioned, the behaviour of the synchrotron flux that steadily decreases as the redshift increases is due to the increased radiative cooling that forces the high-energy tail of $N(\gamma)$ to decrease (see the bottom panel of Fig. 1). We also notice that, even in our simple case of a single power-law injection, the resulting $N(\gamma)$ can be described as a broken power law, breaking at the energy that corresponds to the two peaks of the SED. This corresponds to the Lorentz factor for which $\dot{\gamma}_{\mathrm{ad}} = \dot{\gamma}_{\mathrm{rad}}$ (i.e. $\gamma \sim 2.8 \times 10^4$ for $z = 1$, $\gamma \sim 550$ for $z = 5$, cf. equation 2). The location of the peaks shifts to lower frequencies as the redshift increases, due to the increased cooling, making $N(\gamma)$ to break at lower energies, (see the bottom panel of Fig. 1).

Fig. 2 shows the same SEDs of Fig. 1, but in the observer frame. We report for comparison a limiting sensitivity of 1 mJy at all radio frequencies, and the limiting sensitivity of the Low-Frequency Array (LOFAR; see e.g. van Haarlem et al. 2013), in order to assess the detectability of extended radio sources at high redshifts. Our ideal source could be detected at 1 GHz above 1 mJy up to $z \sim 3$. To push detection further away, we need a better sensitivity: LOFAR can detect these sources at intermediate radio frequencies up to $z \sim 5$. We remind that the plotted fluxes refer only to the *isotropic, extended* emission, thus neglecting the beamed jet emission altogether.

Figure 1. Top panel: SEDs in the rest frame for different redshifts, as labelled. The size of the source is 100 kpc. Particles are injected with a single power-law distribution ($s = 2.3$) and the magnetic field is $B = 10\,\mu$G. Bottom panel: electron energy distribution, plotted in the form $\gamma^3\tau(\gamma)$ as a function of γ, where $\tau(\gamma) \equiv \sigma_T R N(\gamma)$. In this representation, the peak of $\gamma^3\tau(\gamma)$ corresponds to electrons emitting at the peak of the SED.

2.4.2 Double power-law injection

Here, we assume the same parameters as in the previous case, but the injected particle distribution $Q(\gamma)$ is assumed to be a (smoothly joining) double power law:

$$Q(\gamma) = Q_0 \frac{(\gamma/\gamma_b)^{-s_1}}{1 + (\gamma/\gamma_b)^{-s_1+s_2}} \quad (\text{cm}^{-3}\,\text{s}^{-1}). \quad (14)$$

Figs 3 and 4 show the results of assuming $s_1 = 0$, $s_2 = 2.5$ and a break Lorentz factor $\gamma_b = 100$. The $Q(\gamma)$ distribution extends between $\gamma_{\min} \sim 1$ and $\gamma_{\max} \sim 10^7$. In the case of $B = 10\,\mu$G, electrons and magnetic field attain nearly equipartition at $z = 0.1$, where $\log(E_B/\text{erg}) = 59.8$ and $\log(E_e/\text{erg}) = 59.7$. At the same redshift, for $B = 30\,\mu$G, the source is instead magnetically dominated, as $\log(E_B/\text{erg}) = 60.75$ and $\log(E_e/\text{erg}) = 59.4$.

Fig. 4 shows the same SEDs of Fig. 3, but in the observed frame. In the $B = 10\,\mu$G case, an extended source becomes undetectable by LOFAR in the 100 MHz–1 GHz band at $z \gtrsim 5$. The general behaviour is similar to the single power-law case: the Compton
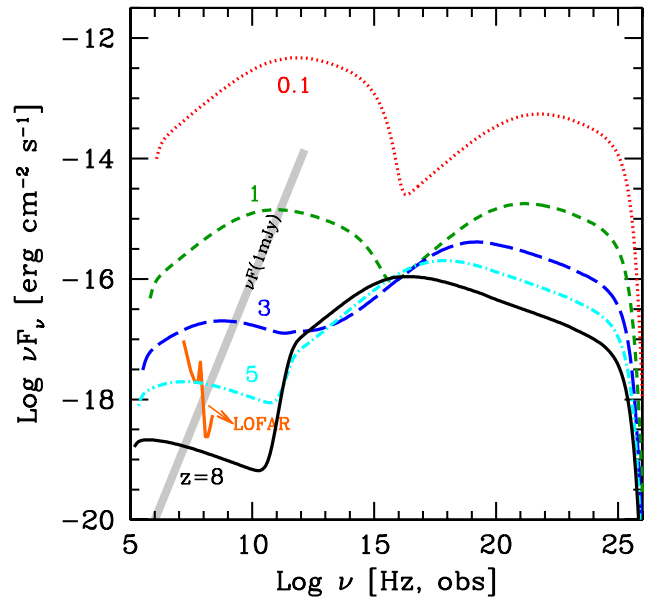
Figure 2. The same as in Fig. 1, but in the observer frame. For illustration, we show the line corresponding to $F(\nu) = 1$ mJy and the limiting sensitivity of LOFAR, once completed. The FIRST survey, corresponding to 1 mJy at the observed frequency of 1.4 GHz, can detect the source up to $z \sim 3$, but not beyond.

dominance increases with z, and at the same time the peaks shift to lower frequencies due to the increase in Compton cooling.
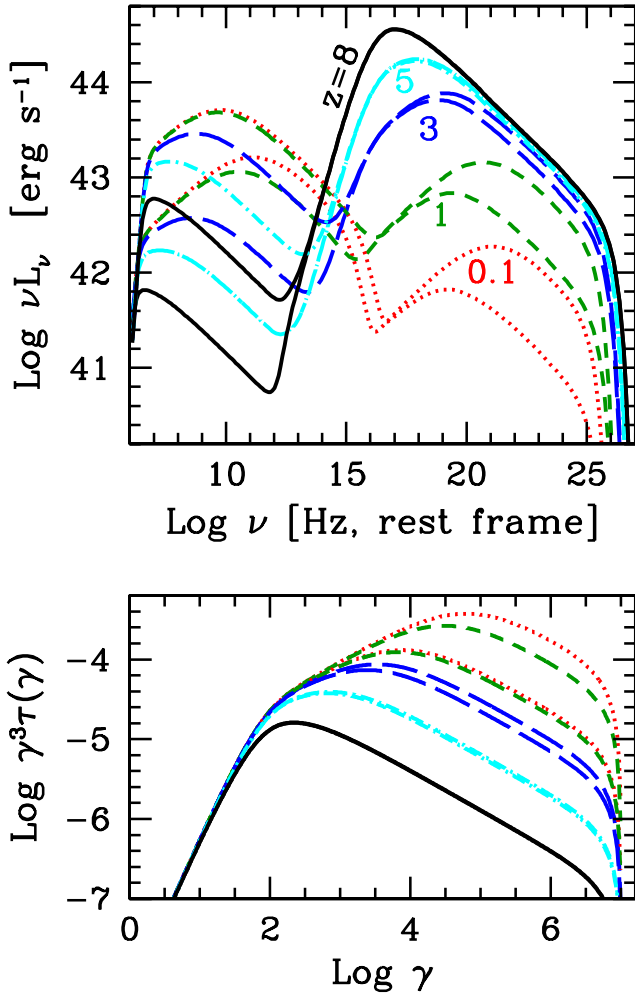
At low redshifts, $z \lesssim 1$, the cooling frequency exceeds the break frequency ν_b (corresponding to γ_b, equation 14), and the SED shows two distinct breaks in the synchrotron-dominated range. The cooling frequency becomes smaller than ν_b at higher redshifts, and a single break, corresponding to the νF_ν peak of the synchrotron emission, is hence featured.

2.4.3 Changing the source size

In order to test the role of the source size, i.e. the escape time-scale, we considered models where $R = 25$ kpc, a quarter of what previously assumed. Fig. 5 shows the SED for a magnetic field $B = 10\,\mu$G, with all the other parameters as in the double power-law models shown in Figs 3 and 4. The top panel illustrates the SEDs in the rest frame of the source, while the bottom panel reports the same SEDs as observed at $z = 0$. Differently from the $R = 100$ kpc case, we note that in a range of (low) radio frequencies, the thin synchrotron luminosity is redshift independent (see top panel, models from $z = 0.1$ to $z \sim 5$), while the luminosity differs at different redshifts above the peak frequency. This implies that if two similar sources located at different redshift are observed above – say – 10 GHz, high-z extended source might be so faint to be undetectable, while observing at – say – 100 MHz both would be visible and with similar luminosities. This offers a clear opportunity to test the CMB effect on extended radio sources as proposed here, by using, e.g. LOFAR.

3 DISCUSSION AND CONCLUSIONS

Beaming makes blazars a unique tool in assessing the number density of radio-loud AGN hosting supermassive BH at high redshift. Indeed, for any confirmed high-redshift blazar there must exist other $\sim 2\Gamma^2 = 450(\Gamma/15)^2$ sources sharing the same intrinsic properties,
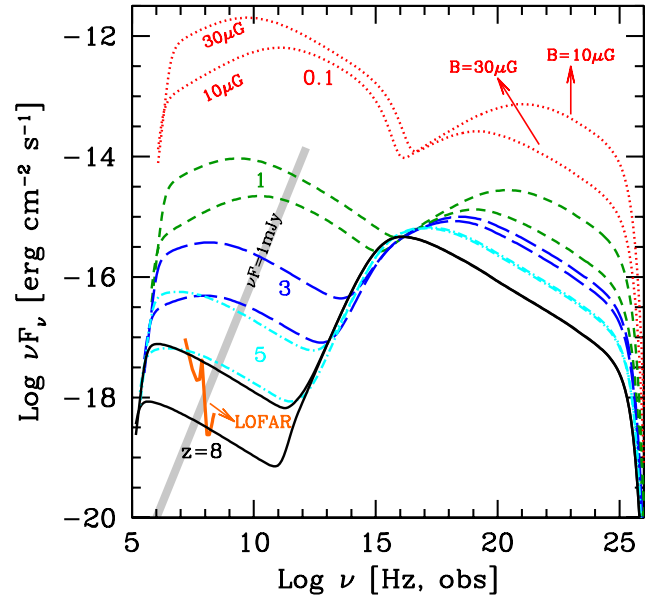
Figure 4. SEDs corresponding to the cases shown in Fig. 3 in the observer frame. For each redshift, two models are shown, for a magnetic field of 10 and 30 μG. A greater magnetic field implies a brighter synchrotron and a fainter IC flux. For illustration, we show the line corresponding to 1 mJy and the limiting sensitivity of LOFAR, once completed.

Figure 3. Top panel: SEDs in the rest frame for different redshifts, as labelled, for a double power-law injections distribution ($s_1 = 0$, $s_2 = 2.5$). The size of the source is 100 kpc. Bottom panel: corresponding electron energy distributions. Solid lines: $B = 10\,\mu G$; dashed lines: $B = 30\,\mu G$.

whose jets are simply not pointing at us. In Ghisellini et al. (2010b) and Volonteri et al. (2011), this idea was exploited to show that the comoving number density of supermassive BHs ($M > 10^9\,M_\odot$) powering *Swift*/BAT (Gehrels et al. 2004) blazars peaks at $z \simeq 4$ (see also Ajello et al. 2009).

The obvious question that followed concerned the observable properties of the hypothetically large parent population of (misaligned) radio galaxies at high redshift. Indeed, such large population may be largely missed in existing radio surveys. Here, we have discussed how the interaction between the electrons and the redshift-dependent CMB energy density affects the emission of extended structures, making the appearance of intrinsically similar radio-loud AGNs different at different cosmic epochs. Our findings can be summarized as follows.

(i) For $z \gtrsim 3$–5, the CMB energy density becomes dominant and partly suppresses the synchrotron flux in extended radio sources. This implies that the spectral properties and the statistics of radio galaxies at high redshifts could be very different from their low-z counterparts.

(ii) We do not expect the radio lobes to be homogeneous, in terms of particle density and magnetic field. In regions where the magnetic

field energy density is larger than the CMB one, $U_B > U_{CMB}$, the electrons are bound to cool down by synchrotron emission anyway, and hence are still efficient radio emitters. Among such regions are the so-called hotspots. Therefore, the observed contrast in radio emission between compact, magnetized regions and more extended lobes should increase for increasing redshifts.

(iii) At low enough energies, radiative cooling is inefficient even considering the IC scattering with CMB photons, at all redshifts. Therefore, the luminosity at the corresponding radio frequencies does not depend upon redshifts (all other parameters being equal). This is potentially testable by observing at high and low radio frequencies.

(iv) The decrease of the radio flux due to the increase of IC off CMB photons could have important consequences when searching for radio-loud sources in large samples, because it introduces an obvious selection effect.

(v) If the hotspot is visible, but not the extended lobes, a classical double radio source can be misclassified as two different point-like radio sources at relatively large angular separation. As an example, a linear projected distance of 100 kpc is seen under an angle of 13, 14.3 and 16 arcsec, at $z = 3$, 4 and 5, respectively. Therefore, when cross correlating sources in optical and radio catalogues, we could be missing some identifications just because a given optical source has no radio counterparts within a pre-assigned search radius.

In conclusion, we have shown how enhanced IC cooling of relativistic electron of CMB photons at high redshifts can potentially alter the radio and X-ray emissions of extended structures associated with radio-loud AGNs. This has important consequences for the statistics of distant radio sources. Potentially, radio surveys could miss many high-redshift *misaligned* sources because of the reduced radio flux of their extended components. Instead, in *aligned* sources (i.e. in blazars), the observed flux comes predominantly from the relatively compact jet, whose radio emission is almost unaffected by the CMB. Therefore, blazars become the most powerful proxies
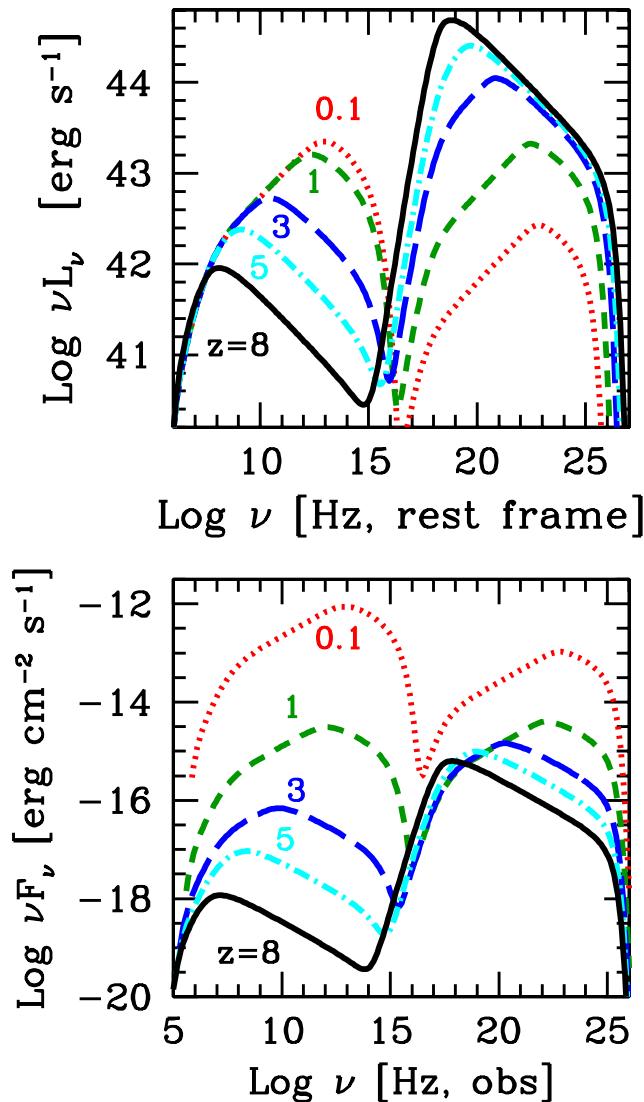
Figure 5. Top panel: as in Fig. 3, but with a source size $R \sim 25$ kpc. The magnetic field is 10 μG. Below the cooling synchrotron frequency, the radio luminosity is independent of redshift, i.e. it is not affected by the increased $U_{\rm CMB}$. At high radio-mm frequencies instead (above the cooling frequencies) the luminosity decreases as z increases. Bottom panel: the same SEDs in the observer frame.

to estimate the distribution and number density of the total (i.e. parent) population of radio sources and to assess the number density of the associated heavy BHs.

REFERENCES

Ajello M. et al., 2009, ApJ, 699, 603
Begelman M. C., Blandford R. D., Rees M. J., 1984, Rev. Mod. Phys., 56, 255
Belsole E., Worrall D. M., Hardcastle M. J., Croston J. H., 2007, MNRAS, 381, 1109
Blandford R., Rees M. J., 1978, in Wolfe A. M., ed., Pittsburgh Conference on BL Lac Objects. Univ. Pittsburgh, Pittsburgh, p. 328
Blundell K. M., Rawlings S., 2000, AJ, 119, 1111
Calderone G., Ghisellini G., Colpi M., Dotti M., 2013, MNRAS, 431, 210
Carilli C. L., Taylor G. B., 2002, ARA&A, 40, 319
Castignani G., Haardt F., Lapi A., De Zotti G., Celotti A., Danese L., 2013, A&A, 560, A28
Celotti A., Fabian A. C., 2004, MNRAS, 353, 523
Celotti A., Ghisellini G., 2008, MNRAS, 385, 283
Croston J. H., Hardcastle M. J., Harris D. E., Belsole E., Birkinshaw M., Worrall D. M., 2005, ApJ, 626, 733
de Young D. S., 2002, The Physics of Extragalactic Radio Sources. Univ. Chicago Press, Chicago, IL
Donato D., Ghisellini G., Tagliaferri G., Fossati G., 2001, A&A, 375, 739
Fanaroff B. L., Riley J. M., 1974, MNRAS, 167, P31
Felten J. E., Rees M. J., 1967, Nature, 221, 924
Fernandes C. A. C. et al., 2011, MNRAS, 411, 1909
Fossati G., Maraschi L., Celotti A., Comastri A., Ghisellini G., 1998, MNRAS, 299, 433
Gehrels N. et al., 2004, ApJ, 611, 1005
Ghisellini G., Celotti A., Fossati G., Maraschi L., Comastri A., 1998, MNRAS, 301, 451
Ghisellini G., Tavecchio F., Foschini L., Ghirlanda G., Maraschi L., Celotti A., 2010a, MNRAS, 402, 497
Ghisellini G. et al., 2010b, MNRAS, 405, 387
Ghisellini G. et al., 2011, MNRAS, 411, 901
Ghisellini G., Haardt F., Della Ceca R., Volonteri M., Sbarrato T., 2013, MNRAS, 432, 2818
Godfrey L. E. H., Shabala S. S., 2013, ApJ, 767, 12
Kataoka J., Stawarz Ł., 2005, ApJ, 622, 797
Kirk J. G., Duffy P., 1999, J. Phys. G, 25, R163
Krolik J. H., Chen W., 1991, AJ, 102, 1659
Mocz P., Fabian A. C., Blundell K. M., 2011, MNRAS, 413, 1107
Nolan P. L. et al., 2012, ApJS, 199, 31
Rees M. J., Setti G., 1968, Nature, 219, 127
Sarazin C. L., 2008, in Plionis M., López-Cruz O., Hughes D., eds, Lecture Notes in Physics, Vol. 740, A Pan-Chromatic View of Clusters of Galaxies and the Large-Scale Structure. Springer, Dordrecht, p. 1
Sbarrato T. et al., 2012, MNRAS, 426, L91
Sbarrato T. et al., 2013, ApJ, 777, 147
Shakura N. I., Sunyaev R. A., 1973, A&A, 24, 337
Shen Y. et al., 2011, ApJS, 194, 45
Sikora M., Begelman M. C., Rees M. J., 1994, ApJ, 421, 153
Urry C. M., Padovani P., 1995, PASP, 107, 803
van Haarlem M. P. et al., 2013, A&A, 556, A2
Volonteri M., Haardt F., Ghisellini G., Della Ceca R., 2011, MNRAS, 416, 216
White R. L., Becker R. H., Helfand D. J., Gregg M. D., 1997, ApJ, 475, 479
York D. G. et al., 2000, AJ, 120, 1579
Yuan W., Fabian A. C., Celotti A., Jonker P. G., 2003, MNRAS, 346, L7